RSC Advances

ROYAL SOCIETY OF CHEMISTRY

www.rsc.org/advances

Uniform $LaPO_4$:Ce/Tb mesoporous microspheres were prepared by a facile mass production co-precipitation process by conjugating Au nanoparticles. Under UV irradiation, a rapid DOX release was achieved due to the photothermal effect of Au nanoparticles deriving from the overlap of the green emission of Tb^{3+} and the surface plasmon resonance (SPR) band of Au.

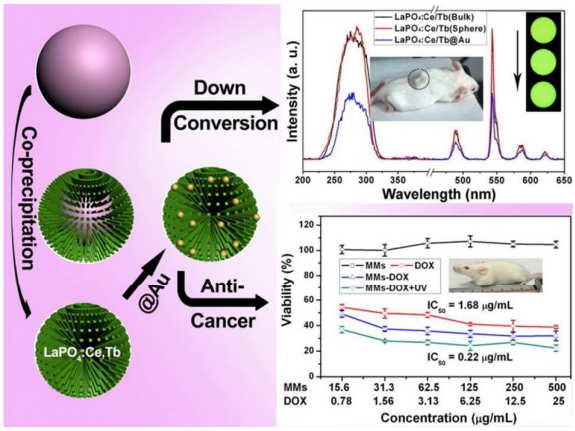

Journal Name

RSCPublishing

ARTICLE

Multifunctional $LaPO_4$:Ce/Tb@Au mesoporous microspheres: synthesis, luminescence and controllable light triggered drug release

Cite this: DOI: 10.1039/x0xx00000x

Received 00th January 2012,
Accepted 00th January 2012

DOI: 10.1039/x0xx00000x

www.rsc.org/

Ruichan Lv, Guixin Yang, Shili Gai*, Yunlu Dai, Fei He, and Piaoping Yang*

Uniform $LaPO_4$:Ce/Tb mesoporous microspheres (MMs) have been successfully prepared by a facile mass production co-precipitation process under mild reaction conditions, without using any surfactant, catalyst and further heating treatment. Then, Au nanoparticles (NPs) were conjugated to polyetherimide (PEI) modified $LaPO_4$:Ce/Tb MMs by the electrostatic interaction. It is found that as-prepared $LaPO_4$:Ce/Tb@Au composite consists of well-dispersed mesoporous microspheres with high surface area and narrow pore size distribution. Upon ultraviolet (UV) excitation, $LaPO_4$:Ce/Tb and $LaPO_4$:Ce/Tb@Au MMs exhibit the characteristic green emissions of Tb^{3+} ions. In addition, the good biocompatibility and sustained doxorubicin (DOX) release properties indicate its promising candidate in cancer therapy. In particular, under UV irradiation, a rapid DOX release was achieved due to the photothermal effect of Au NPs deriving from the overlap of the green emission of Tb^{3+} and the surface plasmon resonance (SPR) band of gold NPs at about 530 nm. The MTT assay, cellular uptaken images, the anti-tumor therapy *in vivo*, and the histology examination results further proved this novel multifunctional (mesoporous, luminescent, and thermal effect) drug delivery system should be a suitable candidate for cancer therapy carriers.

1. Introduction

In recent decades, rare-earth orthophosphates ($REPO_4$) have attracted great attention because of their good photochemical stability, high quantum yield and low toxicity.[1] As luminescence or laser materials, the excellent luminescent properties are mainly based on their particular 4f-5d and 4f-4f electronic transitions which can generate intense and narrow emission bands.[2] Among various $REPO_4$, lanthanum phosphate ($LaPO_4$) with low toxicity and desirable luminescent functions could be potentially applied in the biological field. Meanwhile, mesoporous nano/microspheres with functional properties have also aroused interest because they were widely used as the most promising functional material in various biological fields such as drug carrier,[3] cell imaging,[4] photodynamic therapy,[5] and gene delivery[6] which is due to their distinct low density, high specific surface area and particular porous channel structure.[7] However, rare earth doped $LaPO_4$ mesoporous nano/microspheres employed in the biological applications have rarely been investigated.

The shape control of the as-prepared materials has always been the topic in chemistry materials field. It is well known there is a close relationship between the phase, structure, morphology and their properties in functional materials. Hence, a large number of routes have been reported to fabricate $LaPO_4$ and relative products with various morphology and phase, such as combustion synthesis,[8] solid state method,[9] hydrothermal process,[10] sol-gel process,[11] ultrasonic irradiation,[12] electro-spinning,[13] and chemical co-precipitation method.[14] Among all the methods, the wet chemistry methods have attracted extensive attention because the as-synthesized samples with narrow size distribution and high purity through a mild reaction condition have good performance. Especially, the co-precipitation procedure has superior characteristics to the conventional hydrothermal method, such as simple facilities, lower reaction cost and especially higher yield without using high temperature or pressure. In this regard, the co-precipitation method as a large-scale and facile approach to synthesize the porous materials with functional materials is highly desirable to research.

$LaPO_4$, as an important kind of luminescent host, of which Ce^{3+}/Tb^{3+} co-activated and Eu^{3+}-doped bulk powders were extensively applied as the green and red phosphors.[15] Song *et al.* compared the luminescent properties of Ce^{3+}/Tb^{3+} co-activated and Eu^{3+} activated $LaPO_4$ with different structures of nano/micro-wires, nano/microrods and nano/microspheres.[16] They concluded that the nanowires/rods had higher quantum efficiency and higher electronic transition rate due to the shape anisotropy, while the micro-particles exhibited higher radiative transition rate because of the improved surface-to-volume ratio. Recent research has also attempted to design new structures in order to regulate the fluorescent properties including the intensity and lifetime.[17]

Drug delivery systems (DDSs) have widely been studied because rapid large dosage could cause severe side effects to normal tissues. The key ability of DDSs is to regulate drug release, minimize side effects and improve therapeutic efficacy

of conventional pharmaceuticals.[18] In general, endogenous and exogenous activation are the two approaches used to regulate the release of the therapeutic payload. The important benefit of exogenous control is to externally regulate drug dosing simply. It is meaningful to find activations which could provide a highly orthogonal external stimulus, allowing spatiotemporal control of payload release. Compared to the widely used fluorescent dyes and quantum dots, gold NPs have unique properties such as good chemical and photo stability, ease of synthesis, and facile conjugation.[19] Meanwhile, lanthanides with excellent luminescent properties could widely be used in the therapeutic efficacy as drug carrier. The combination of the two materials may induce the photothermal effect due to SPR effect which could be potentially used to control the drug release process. Therefore, multifunctional lanthanide-gold composite should be highly desirable which hold the possibility to control the released efficiency through regulating exogenous conditions.[20]

In this study, we designed a facile and mild co-precipitation method to prepare $LaPO_4$:Ce/Tb microspheres with mesoporous structure which are assembled by numerous hexagonal nano-rods. Au NPs with the average size of about 10 nm were conjugated to PEI modified $LaPO_4$:Ce/Tb MMs to obtain a multifunctional drug carrier. Down-conversion properties were studied to evaluate the luminescent properties of $LaPO_4$:Ce/Tb and $LaPO_4$:Ce/Tb@Au MMs. In addition, MTT assay and DOX released properties of $LaPO_4$:Ce/Tb@Au MMs were studied to evaluate the feasibility of this functional composite as the potential drug carrier. Meanwhile, the viability of L929 cells *in vitro*, the hemolysis assay of human red blood, the toxicity under different conditions, and the inverted fluorescence microscope images uptaken by cancer cells of $LaPO_4$:Ce/Tb@Au were also measured. The final anti-cancer properties *in vivo* and the histology examination proved the potential candidate as anti-cancer drug carrier with bio-imaging.

2. Experimental section

2.1. Reagents and materials

All of the chemical reagents used in this experiment are of analytical grade without any further purification, including urea, hydrochloric acid (HCl), ammonium secondary phosphate ($NH_4H_2PO_4$), ammonium hydroxide (NH_4OH), sodium citrate, tannic acid, chloroauric acid ($HAuCl_4$) (Beijing Chemical Corporation), La_2O_3 (99.99%), Ce_2O_3, and Tb_4O_7 (99.99%) (Sinopharm Chemical Reagent Co., Ltd.), PEI, phosphate buffered saline (PBS), and potassium hydrogen phthalate (PHP), dimethyl sulfoxide (DMSO), 3-[4,5-dimethylthiazol-2-yl]-2,5-diphenyl tetrazolium bromide (MTT), DOX (Tianjin Kermel Chemical Reagent Co., Ltd.).

2.2. Synthesis, MTT assay and DOX release

Synthesis of $La(OH)CO_3$:Ce/Tb microspheres. $La(OH)CO_3$ microspheres were prepared *via* urea-based precipitation process. In a typical process, 0.5 M $LaCl_3$ was prepared by dissolving corresponding calculated La_2O_3 into HCl with gradually heating. A total of 0.5 mL of 1.0 M $LaCl_3$ and 1.5 g of urea were dissolved to 50 mL deionized water in a beaker. After stirred for 5 min, the mixture was kept heating at 90 °C for 3 h through water bath. The resulting mixture was centrifuged at 6000 rpm for 4 min. The supernatant solution was discarded, and the precipitate was saved with fresh deionized water. After this process was repeated three times, $La(OH)CO_3$ microspheres were acquired. The preparation of $La(OH)CO_3$:Ce/Tb microspheres was similar to the procedure above with La: Ce: Tb molar ratio of 85: 10: 5.

Synthesis of $LaPO_4$:Ce/Tb MMs. The as-prepared 0.5 mmol of $La(OH)CO_3$:Ce/Tb sample was dissolved by 10 mL deionized water, and then 1 mmol $NH_4H_2PO_4$ was added without regulating the pH value with continuous stirring. The beaker was then transferred to the water bath kettle at 90 °C. After 3 h of reaction, the resulting product was centrifuged three times and dried in the baking oven for 12 h to obtain $LaPO_4$:Ce/Tb. For comparison, bulk $LaPO_4$:Ce/Tb was directly co-precipitated by $Ln(NO_3)_3$ (Ln = La: Ce: Tb, with molar ratio of 85: 10: 5) (0.5 mmol) and $NH_4H_2PO_4$ (0.5 mmol) at 90 °C for 3 h. $LaPO_4$:Ce/Tb samples with varying pH value are regulated by HCl and NH_4OH. Samples prepared with pH values of 3, 6.5, and 10 are marked as Sample-3, Sample-6.5, and Sample-10.

Synthesis of $LaPO_4$:Ce/Tb@Au. The gold NPs with a diameter of about 10 nm were prepared by the citrate reduction method in the presence of tannic acid as reducing agent.[21] Typically, 5 mL of 1 g/L $HAuCl_4$ was mixed with 30 mL deionized water containing 0.2 g sodium citrate and 0.03 g tannic acid and kept at 60 °C for 4 h. Then, the as-prepared $LaPO_4$:Ce/Tb MMs were dispersed in 20 mL of water containing 0.1 g PEI and stirred for 2 h. The PEI modified $LaPO_4$:Ce/Tb were collected by centrifugation, washed by deionized water, and re-dispersed in 20 mL deionized water. Consequently, 1 mL of the as-prepared gold suspension was swiftly added into above solution, and slowly rotated for 2 h, the $LaPO_4$:Ce/Tb@Au microspheres were collected by centrifugation.

***In vitro* viability of $LaPO_4$:Ce/Tb@Au.** 5000-6000 L929 fibroblast cells were plated in 200 mL media per well in a 96-well plate, and 8 wells were left empty for blank control, then incubated 24 h to allow the cells to attach to the wells at 37 °C with 5% CO_2. The $LaPO_4$:Ce/Tb@Au spheres were sterilized via ultraviolet irradiation for 2 h, and then diluting at concentrations of 15.63, 31.25, 62.5, 125, 250, and 500 μg/mL, respectively. The solution with different concentration was added to the wells and incubated for another 24 h at 37 °C with 5% CO_2. Then 5 mg/mL MTT solution was prepared by PBS. 20 μL solution was added to each well containing different amounts of $LaPO_4$:Ce/Tb@Au. The plate was incubated at 37 °C for another 4 h subsequently. During this period, viable cells make MTT reduce into formazan, which can be dissolved by DMSO. After incubation, the 96-well plate was placed on a shaking table for 5 min of 150 rpm in order to make the formazan and solvent mixed completely. The absorbance of the suspension was recorded using a microplate reader (Therom Multiskan MK3) regulating to 490 nm as detecting wavelength. Optical density which received no polymer or drug was considered as 100% growth.

Hemolysis Assay. Red blood cells were acquired by removing the serum from the EDTA.K2 stabilized human blood through washing with 1% normal saline, and centrifugated several times until the supernatant were transparent. Then, the blood cells were diluted to 1/10 with PBS solution (pH = 7.4). Diluted cells suspension (0.4 mL) was then mixed with: (1) 1.6 mL of PBS as a negative control; (2) 1.6 mL of deionized water as a positive control; and (3) 1.6 mL of materials suspensions with varying concentration (15.63, 31.25, 62.5, 125, 250, and 500 μg/mL). The ten samples were shaken and kept stable for 2 h at room temperature. Finally, the mixtures were centrifuged and the absorbance of the upper supernatants was measured by

UV-vis. The percentage of hemolysis was calculated using the following equation: Hemolysis % = (A_{sample} - $A_{control(-)}$) / ($A_{control(+)}$ - $A_{control(-)}$), where A is the absorbance of UV-vis spectrum.

DOX loading and release test. 0.03 g $LaPO_4$:Ce/Tb and $LaPO_4$:Ce/Tb@Au sample was added into 10 mL of phosphate buffered saline (PBS) and ultrasonic dispersed, respectively. After that, 2.5 mg DOX was added into the solution with slow stirring at room temperature for 24 h. The as-prepared mixture was centrifugally separated at 6000 rpm for 4 min for three times, then the supernatant solution was kept for ultraviolet visible light analysis. 10 mL fresh PBS was replenished in the centrifugal tube, the $LaPO_4$:Ce/Tb@Au solution under investigation was irradiated by the UV lamp in a 1 cm length quartz cuvette. During the released period, the comparative samples (with or without irradiation) were shaken together for 1 min at one hour interval. After centrifugation, the supernatant solution was kept. The process was repeated and changed release time (60 min, 2 h, 4 h, 6 h, 8 h, 12 h, 24 h and 32 h, *etc*), respectively. PBS (pH = 7) and PHP (pH = 4) was prepared directly by pH modifier. The mass of the released DOX was obtained by the absorbance with the specified 480 nm which is shown Fig. S1. The loading amount (M_{LA}) can be calculated using the formula: $M_{LA} = O_{DOX} - R_{DOX}$ where O_{DOX} is the original DOX concentration and R_{DOX} is the residual concentration. The loading efficiency (LE %) can be calculated using the formula: $LE = M_{LA} / O_{DOX}$. The release efficiency (RE %) can be calculated using the formula: $RE = \Sigma M_{DOX\ in\ supermatant} / M_{LA}$. where $M_{DOX\ in\ supermatant}$ is the DOX concentration in the supernatant with different released time)

***In vitro* cytotoxicity of $LaPO_4$:Ce/Tb@Au.** HeLa cells were plated out in 96-well plates at a density of 8000 cells per well and grew overnight to make cells attached. The cells were incubated in 5 % CO_2 at 37 °C for 24 h, and then $LaPO_4$:Ce/Tb@Au, DOX-$LaPO_4$:Ce/Tb@Au and DOX were added to the medium. The concentrations of DOX are regulated to 0.78, 1.56, 3.13, 6.25, 12.5, and 25 μg/mL, respectively. The concentrations of $LaPO_4$:Ce/Tb@Au are 15.6, 31.3, 62.5, 125, 250, and 500 μg/mL, respectively. UV irradiation was used for 30 min using a UV lamp with the pump power of 0.2 W/cm^2. At the end of the incubation process, 20 μL of MTT solution was added into each cell and incubated for another 4 h. The supernatant in each well was aspirated and 150 μL of DMSO was added before the plate was examined using a microplate reader at the wavelength of 490 nm.

Cellular uptake. Cellular uptake by HeLa cancer cells was detected using a confocal laser scanning microscope (CLSM, Leica TCS SP8). HeLa cells were seeded in a 6-well culture plate and grown at 37 °C overnight. After that, the HeLa cells were incubated with $LaPO_4$:Ce/Tb@Au-DOX at 37 °C for 0.5 h, 3 h, and 6 h, respectively. Then, the cells were rinsed with PBS three times, and fixed with 2.5% formaldehyde (1 mL/well) at 37 °C for 10 min, and rinsed again with PBS three times. The nuclei were dyed with DAPI solution (20 μg/mL in PBS, 1 mL/well) for 10 min for labeling the nucleus. After that, the cells were rinsed with PBS three times.

***In Vivo* Toxicity of $LaPO_4$:Ce/Tb@Au-DOX.** Female Kunming mice (25-35 g) were purchased from Harbin Veterinary Research Institute, Chinese Academy of Agricultural Sciences (Harbin, China), and all the mouse experiments were performed in compliance with the criterions of The National Regulation of China for Care and Use of Laboratory Animals. Firstly, the tumors were established by subcutaneous injection of H22 cells (murine hepatocarcinoma cell lines) in the left axilla of each female mouse. After grown for 1 week, the tumors sizes reached the size about 6-8 mm. The tumor-bearing mice were randomized into 3 groups (n = 5, each group) and were treated by intratumor injection with nothing, pure DOX, and $LaPO_4$:Ce/Tb@Au+DOX with UV laser irradiation. The first group were made for blank control without any injected. The injected material is 100 μL (1 mg/mL) every two days, and pure DOX is 50 μL (1 mg/mL) were consistent with the materials.

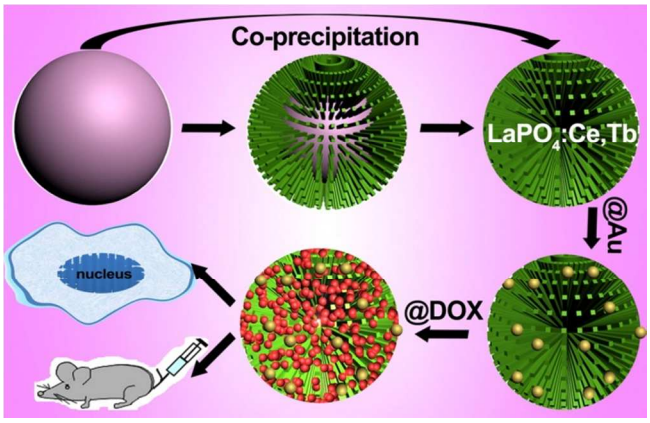

Scheme 1 The schematic diagram for the formation of $LaPO_4$:Ce/Tb and $LaPO_4$:Ce/Tb@Au MMs and drug loading/release process.

Histology Examination. Histology analysis was performed at the 14th day after treatment. The typical heart, liver, spleen, lung, and kidney tissues of the mice in the control group and treatment group were isolated. After that, the organs dehydrated using buffered formalin, ethanol with different concentrations, xylene. Then, they were embedded in liquid paraffin. The sliced organs and tumor tissues (3-5 mm) were stained with Hematoxylin and Eosin (H&E) and examined by a microscope.

2.3. Characterization

Powder X-ray diffraction (XRD) measurements were performed on a Rigaku D/max TTR-III diffractometer at a scanning rate of 15°/min in the 2θ range from 20° to 80°, with graphite monochromatized Cu Kα radiation (λ = 0.15405 nm). Images were obtained digitally on scanning electron microscope (SEM, JSM-6480A), transmission electron microscopy (TEM, FEI Tecnai G^2 S-Twin) and high-resolution transmission electron microscopy (HRTEM). Fourier Transform Infrared Spectroscopy (FT-IR) spectra were measured on a Perkin-Elmer 580B IR spectrophotometer using the KBr pellet technique. N_2 adsorption/desorption isotherms were obtained on a Micromeritics ASAP 2010 apparatus. The photoluminescence were excited by a 150 W Xenon lamp. DOX concentration and the absorbance of gold NPs solution were detected by UV-1601 spectrophotometer. The measurements were all performed at room temperature.

3. Results and discussion

The procedure for the formation of luminescent $LaPO_4$:Ce/Tb microspheres, $LaPO_4$:Ce/Tb@Au microspheres and further drug loading and release process is presented in Scheme 1. It is well known that low doping amount does not change the phase or morphology of the final product due to the much similar ion radius of the doped rare earth ions. XRD patterns of $LaPO_4$ and $LaPO_4$:Ce/Tb are given in Fig. S2. We can see the patterns of the two samples are almost similar. No additional peaks of

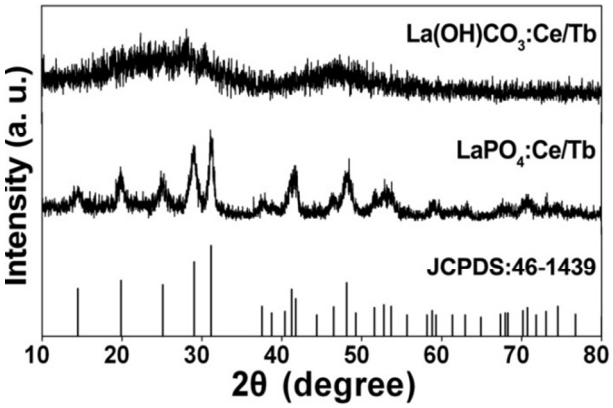

Fig. 1 XRD patterns of $La(OH)CO_3$:Ce/Tb precursor and $LaPO_4$:Ce/Tb MMs.

other phases have been found, indicating that the other lanthanide ions have been successfully doped into the hexagonal phase of $LaPO_4$ host lattice.

3.1. Phase, structure and morphology

Fig. 1 shows the XRD patterns of the co-precipitated precursor $La(OH)CO_3$:Ce/Tb and the resulting product $LaPO_4$:Ce/Tb. The diffraction peaks of the precursor can be indexed to orthorhombic $La(OH)CO_3$ (JCPDS No. 49–0981). Meanwhile, the XRD pattern shows broad bands, which indicates that the precursor is amorphous. The diffractions of the resulted product are in good agreement with the hexagonal-phased $LaPO_4$ (JCPDS No. 46–1439). The sharp and strong peaks indicate the pure phase and high crystallinity of the resulting product $LaPO_4$:Ce/Tb.

A typical TEM image of the precursor $La(OH)CO_3$:Ce/Tb is shown in Fig. S3, it reveals the sample is well dispersed and consists of microspheres with an average diameter of 180 nm. The high dispersibility of the precursor is favorable to obtain

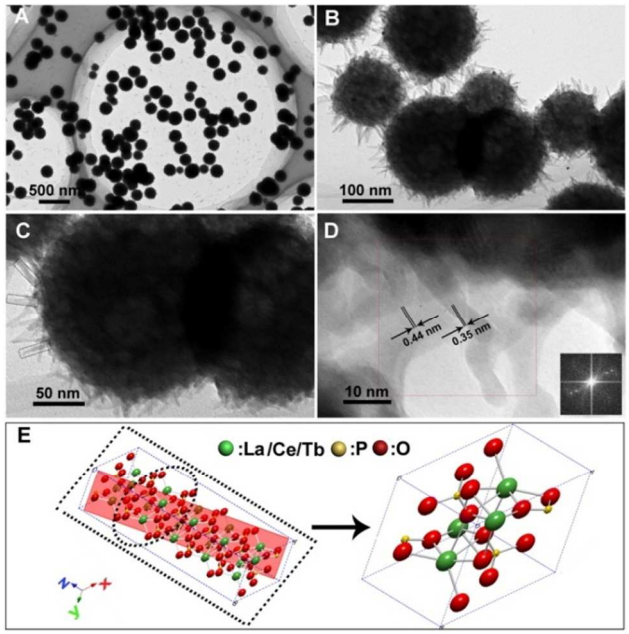

Fig. 2 TEM images with different magnifications (A-C), HRTEM image (D) and schematic crystal structure diagrams (E) of $LaPO_4$:Ce/Tb MMs.

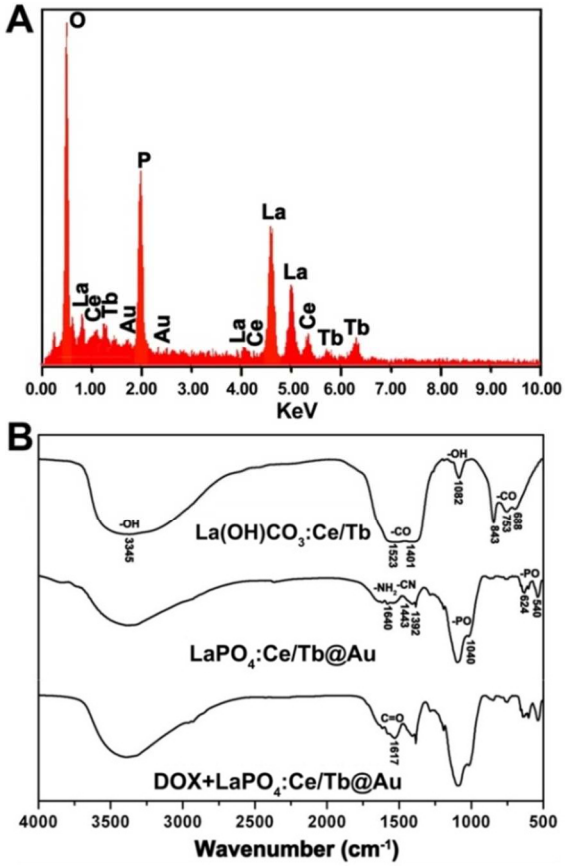

Fig. 3 EDS of $LaPO_4$:Ce/Tb@Au MMs (A), FT-IR spectra of the precursor $La(OH)CO_3$:Ce/Tb, the resulted $LaPO_4$:Ce/Tb@Au, and DOX loaded $LaPO_4$:Ce/Tb@Au (B).

uniform final products. After the co-precipitation of the precursor with $NH_4H_2PO_4$ for 3 h at 90 °C, $LaPO_4$:Ce/Tb porous microspheres can be obtained. TEM images (Fig. 2A, B) indicate the product is composed of well dispersed porous spheres with diameter of 160 nm to 190 nm, which is much similar to those of original precursor in shape and size (Fig. S3). High-magnified TEM images (Fig. 2C) show that the product is constituted with numerous nanorods, which has a diameter of 3-5 nm and a height of 20-40 nm. This is well consistent with the reported literature,[16] and this structure favors the luminescent property, which will be discussed in the next section. The HRTEM image (Fig. 2D) shows the obvious lattice fringes with adjacent distance of 0.44 nm and 0.35 nm, matching well with the d-spacing of (101) plane and (110) plane for hexagonal phased $LaPO_4$:Ce/Tb. In Fig. 2E, the left one shows the schematic diagram of a nanorod grown along [001] direction. This model responds to the nanorods in Fig. 2C (marked with dotted frame). The right one in Fig. 2E depicts the unit cell in which the La/Ce/Tb atoms (green spheres) is coordinated by nine oxygen atoms (red spheres) and four of oxygen atoms form a distorted tetrahedron that interpenetrates a quasi-planar pentagon formed by the other five.[22]

The two-step synthesis method always faced the problem whether the precursor was completely reacted in the second step. Therefore, it is essential to prove the purity of the resulted product. Here, the EDS and FTIR spectra are used to test the phase of the as-prepare $LaPO_4$:Ce/Tb@Au. The EDS pattern (Fig. 3A) confirms the presence of La, Ce, Tb, Au, P and O in the product. There is no C atoms maintained which confirms

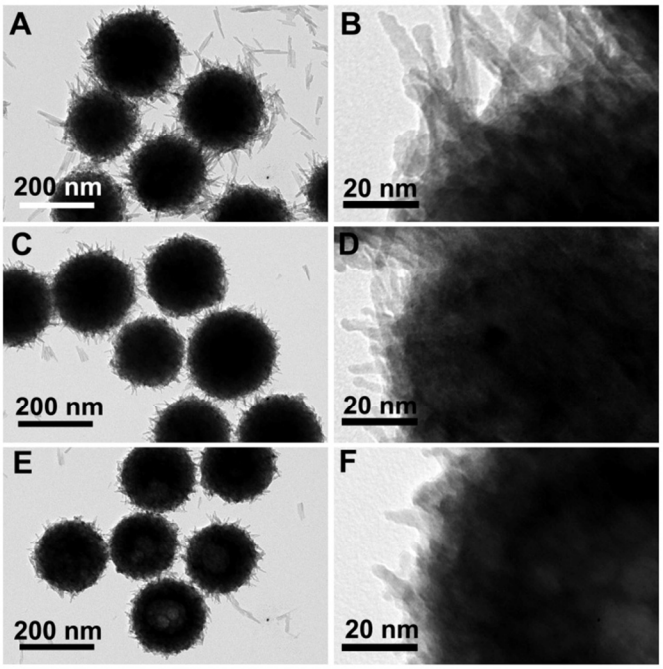

Fig. 4 TEM images of $LaPO_4$:Ce/Tb prepared with the initial pH value of 3 (A and B), 6.5 (C and D), and 10 (E and F).

the purity of the resulted product. FT-IR spectroscopy was conducted for the precursor $La(OH)CO_3$:Ce/Tb, the final $LaPO_4$:Ce/Tb@Au, and $LaPO_4$:Ce/Tb@Au loaded with DOX, as shown in Fig. 3B. A similar band in all three samples at 3345 cm^{-1} and 1082 cm^{-1} is due to the -OH stretching and bending vibrations of water and hydroxyl groups.[23] For the precursor, the characteristic absorption bands of O-C-O (1523 and 1401 cm^{-1}), π-CO_3^{2-} (843 cm^{-1}) and δ-CO_3^{2-} (753 and 688 cm^{-1}) can be observed in the precursor, which indicate the existence of $La(OH)CO_3$:Ce/Tb.[24] The unique absorption peaks at 1640, 1443, and 1392 cm^{-1} are from the internal vibration of $-NH_2$ and –CN which reveals the presence of PEI on the $LaPO_4$:Ce/Tb@Au. And the respective peak at 1040, 624, and 540 cm^{-1} is ascribed to P-O stretching, O=P-O bending and O-P-O bending mode of vibration.[25] For DOX loaded $LaPO_4$:Ce/Tb@Au, the unique band at 1617 cm^{-1} is ascribed to the stretching vibrations of C=O in DOX, providing the additional evidence for the loading of DOX molecules on $LaPO_4$:Ce/Tb@Au porous microspheres.[26]

Fig. 4 shows the effect of the initial pH value on the morphology and the size of the $LaPO_4$:Ce/Tb micro-spheres. All of them are prepared at the temperature of 90 °C for 3 h. From Fig. 4A, C and E, we can see the micro-spheres change from the solid to hollow spheres. The difference was generated from the different dissolution rate between the Ln^{3+} (inside) and PO_4^{3-} (outside) ions. When the initial reaction environment is acid (pH = 3), it is difficult to the hydrolyzation of $H_2PO_4^-$ ions and the co-precipitation of Ln^{3+} and PO_4^{3-} will proceed slowly. When the initial pH value is 10, the precursor dissolved to Ln^{3+} and the $H_2PO_4^-$ hydrolyzed to PO_4^{3-} quickly, then $LaPO_4$ formed in the shell firstly. The shell hindered the further co-precipitation with that the inside Ln^{3+} ions could go through the shell more quickly than the outside PO_4^{3-} ions due to the different ions size. It is known that if the diffusion rate of Ln^{3+} ions from inside to outside is faster than that of F^- from outside, Kirkendall voids will be generated, leading to the formation of

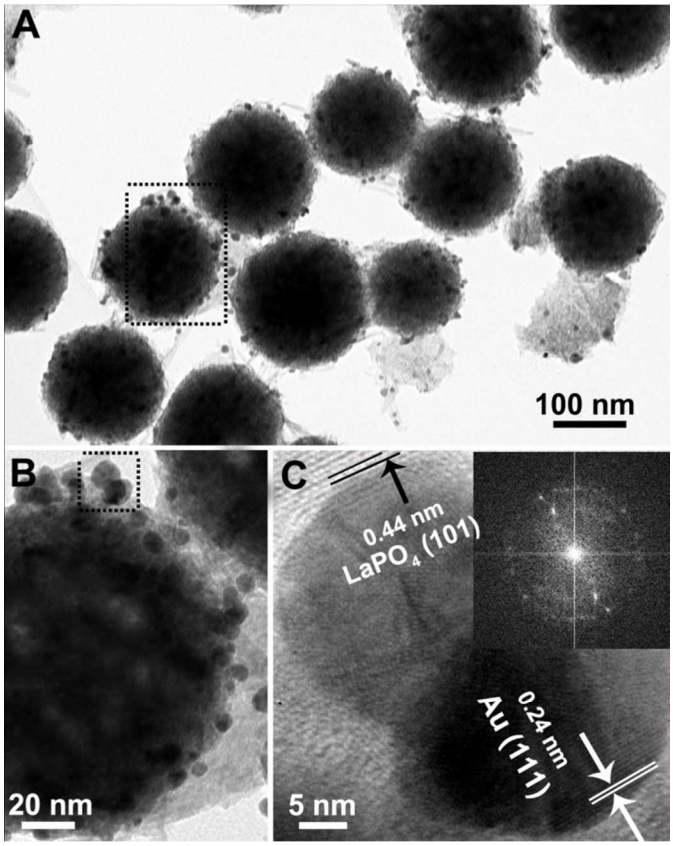

Fig. 5 Low-(A), high-magnified (B), and HRTEM (C) images of $LaPO_4$:Ce/Tb@Au MMs.

hollow spheres. Therefore, the hollow spheres generated when the pH value was 10. Meanwhile, we can see there was a little decrease in the size of the three samples with the increasing pH value which could be attributed to the higher dissolution efficiency of the precursor. From these phenomena, we can also conclude that micro-sphere $LaPO_4$:Ce/Tb generated from outside to inside.

In addition, the sizes of the nano-rods changed among different samples as shown in Fig. 4B, 4D, and 4F. When the pH value is 3, the length of the nano-rods was in an average of 40 nm. The length decreases to 25 nm with the pH value of 6.5 and 15 nm with the pH value of 10. This is due to $H_2PO_4^-$ as a natural surfactant caused the low reaction rate between Ln^{3+} and PO_4^{3-} ions which is favourable to the growth of $LaPO_4$ hexagonal crystals, and then they grew preferentially along the [100] direction.

Before attaching with gold nanoparticles, the surface of $LaPO_4$:Ce/Tb was firstly modified with positively charged PEI, which strongly coordinates with the negatively charged Au NPs. The typical SEM images of the as-prepared $LaPO_4$:Ce/Tb@Au MMs were shown in Fig. S4A-C. Seen from SEM images and TEM image (Fig. 5A), we can conclude the modified PEI has no obvious side effect on the uniformity or aggregation. The diameter distribution programs of the precursor and $LaPO_4$:Ce/Tb@Au are shown in Fig. S4D, which reveal the as-prepared MMs' diameter is well-distributed. The gold NPs (Fig. 5B), we can see that the particle size of the coated gold NPs is about 10 nm. HRTEM in Fig. 5C shows that the apparent lattice fringes with adjacent distance of 0.44 nm,

corresponding to d-spacing of (101) plane for hexagonal phased $LaPO_4$ (JCPDS No.

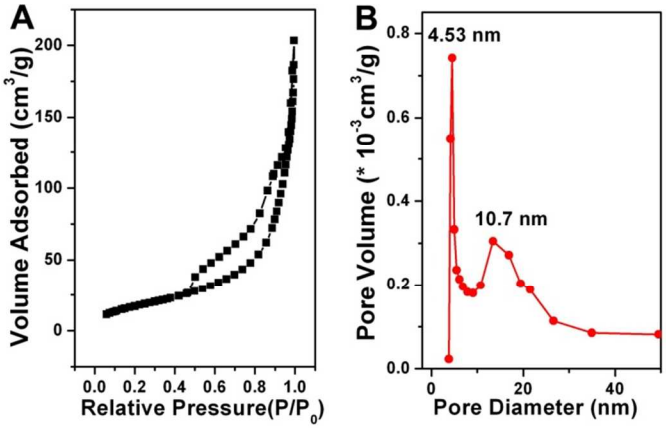

Fig. 6 Nitrogen adsorption/desorption isotherm of $LaPO_4$:Ce/Tb@Au MMs (A), and corresponding pore size distribution curve (B).

46–1439), and the distance of 0.24 nm matches with the interplaner distance of (111) plane for cubic phased Au (JCPDS No. 04–0784).

Nitrogen adsorption/desorption experiment was employed to study the porous structure of $LaPO_4$:Ce/Tb@Au MMs. It can be seen from Fig. 6A that the sample exhibits typical IV-typed isotherms with H1-hysteresis loops, which shows the characteristics of typical mesoporous materials.[27] The BET

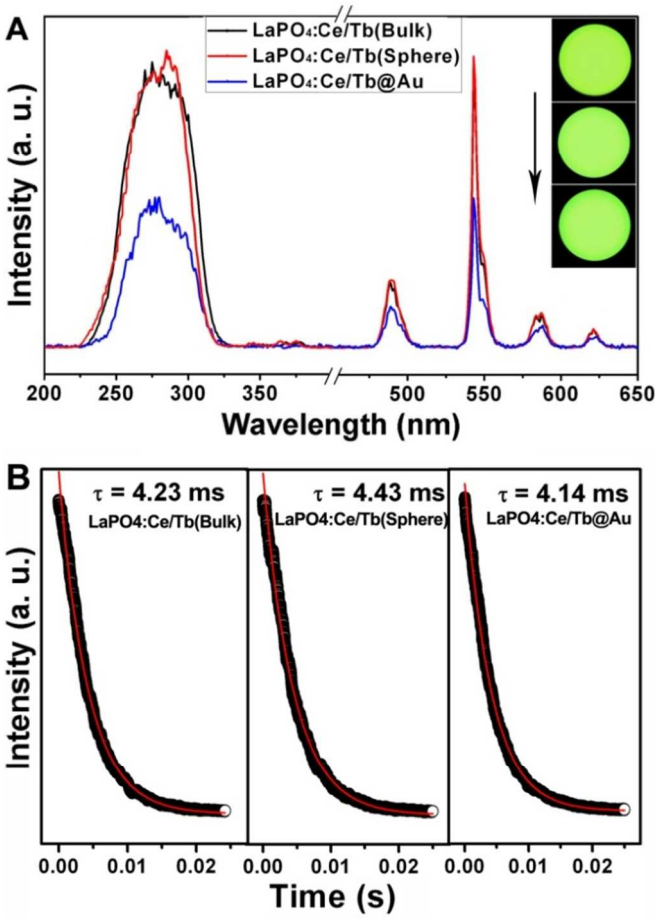

Fig. 7 Excitation (left) and emission (right) spectra (A), and decay curves (B) of bulk $LaPO_4$:Ce/Tb, $LaPO_4$:Ce/Tb MMs, and $LaPO_4$:Ce/Tb@Au MMs. Insets are the corresponding photographs under UV irradiation.

surface area and total pore volume were calculated to be 66 m^2/g and 0.303 cm^3/g. The pore size distribution curves (Fig. 6B) represent the pore sizes with average pore diameters which reveal the sizes of $LaPO_4$:Ce/Tb@Au MMs' pores are irregular with two main kinds of pores (4.53 nm and 10.74 nm). The mesoporous structure with high specific surface area is suitable as drug carrier.[28]

3.2. Photoluminescence properties

The luminescent properties of bulk $LaPO_4$:Ce/Tb, $LaPO_4$:Ce/Tb MMs, and $LaPO_4$:Ce/Tb@Au MMs are given in Fig. 7. As shown, the excitation spectra (Fig. 7A, left) consist of a broad band centered at 276 nm due to the transitions from the ground $^2F_{5/2}$ state to the 5d levels, and several weak peaks between 330-380 nm assigned to f-f transitions of Tb^{3+}.[29] The emission spectra (Fig. 7A, right) all contain four strong peaks (491, 543, 587 and 620 nm), corresponding to the respective f-f transition of Tb^{3+} from the excited $^5D_4$ to the ^7F_J levels (J = 6, 5, 4, 3) levels.[30]

It is apparent that $^5D_4 \rightarrow {}^7F_5$ emission is predominant, which emits bright green emissions (insets in Fig. 7A). It should be noted that $LaPO_4$:Ce/Tb MMs show high emission intensity and long decay time (Fig. 7B), which is even a little higher than that of bulk $LaPO_4$:Ce/Tb powder. The emission ($^5D_4 \rightarrow {}^7F_5$) intensity ratio of $LaPO_4$:Ce/Tb MMs to bulk sample is 1.08:1, while the intensity ratio of $LaPO_4$:Ce/Tb@Au to $LaPO_4$:Ce/Tb MMs is 0.56:1. The results reveal that as-prepared $LaPO_4$:Ce/Tb MMs show high emission intensity, which is due to the unique structure of $LaPO_4$:Ce/Tb microspheres consisting of nanorods. The nanorods have higher quantum efficiency and higher electronic transition rate. Meanwhile, the micro-particles exhibited higher radiative transition rate because of the improved surface-to-volume ratio.[31] The absorption mechanism (absorption and scattering of Au NPs) should result in the suppression of the emission for Au NPs attached product. We can see that the difference of the emission spectra for $LaPO_4$:Ce/Tb and $LaPO_4$:Ce/Tb@Au is mainly focused on the 500-600 nm, which is the absorbance of the Au NPs (as shown in Fig. S5). That means the loss of the luminescent light would be absorbed by non-radiative energy transfer from the phosphor to the metal via the SPR absorption when gold crystals are attached to their surface. In order to further prove the transition between Au NPs and the phosphors, we also tested the decay time of $LaPO_4$:Ce/Tb@Au, which is shown in Fig. 7B. We can see $LaPO_4$:Ce/Tb microspheres have the longer decay time of 4.43 ms than the bulk structure (4.23 ms). Comparing with $LaPO_4$:Ce/Tb, $LaPO_4$:Ce/Tb@Au MMs have a little shorter lifetime (4.14 ms), which also means that less energy has been transferred from excited Ce^{3+} ions to Tb^{3+} ions and thus decreases down-conversion populating processes of Tb^{3+} ions.

3.3. Cell viability, drug release and MTT cytotoxicity assay

For potential biological application, the cell viability of the as-prepared materials is essential to evaluate.[56] Standard MTT cell assay was carried on L929 cell lines to detect the viability of $LaPO_4$:Ce/Tb@Au MMs. Fig. 8A depicts the cell viability with different concentration of $LaPO_4$:Ce/Tb@Au varying from 15.63 to 500 ug/mL incubated for 24 h. It is shown that the biocompatibility of the as-prepared material in all dosages is up

to 95.87%–105.27%. And there is still 105.27% observed even at a high-dose concentration of 500 μg/mL.

To guarantee the potential intravenous administration *in vivo*, it is essential to detect the biocompatibility with red blood cells.

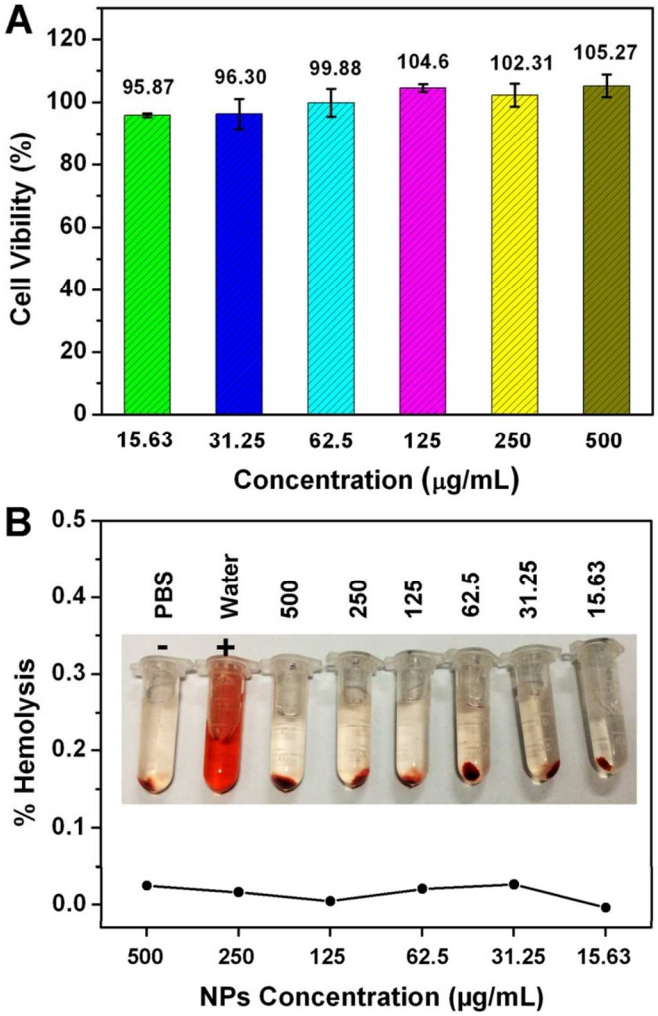

Fig. 8 The viability of L929 fibroblast cell incubated for 24 h (A) and the hemolysis results of human red blood (B) with $LaPO_4$:Ce/Tb@Au MMs of different concentrations.

Fig. 8B presents the hemolytic result, and the red solution inset is attributed to the presence of hemoglobin. There is no visually red colour occurred, which indicates there is negligible hemolysis in the controlled tubes with different solution added. For the obtained red solution (dissolved with H_2O), it is caused by hemolysis because of released hemoglobin into the solution. The highest hemolytic efficiency with different particle concentration from 15.63 to 500 μg mL^{-1} is 0.03%, indicating that the as-prepared $LaPO_4$:Ce/Tb@Au is almost not hemolytic. To sum up, the MTT assay data and hemolysis result demonstrate that this material is nontoxic to live cells and can be proposed to apply in the biotechnology as drug carrier.

Here, DOX was used as a model drug to evaluate the loading and release behavior. And pH values of 4 and 7 were selected as the different values to demonstrate the release efficiency, which usually represents the environment of cancer cell and normal cell, respectively. After continuous stirring for 24 h and centrifugation for three times, DOX has been adsorbed to $LaPO_4$:Ce/Tb@Au with loading efficiency of 61.1% and the loading amount of DOX was 1.53 mg. This result corresponds well to other mesoporous materials released in conditions of different pH values.[32] The N_2 adsorption/desorption of the samples prepared with different pH values and the DOX loading/release properties of the samples (Fig. 4) prepared with different pH values were also studied (Fig. S6). Figure S6A shows that the BET surface areas increase with enhanced initial pH values. After continuous stirring, the loading amount of DOX with Sample-3, Sample-6.5, and Sample-10 is 1.45 mg (57.8%), 1.55 mg (62.0%), and 1.66 mg (66.5%), respectively. As shown in Fig. S6B, with enhanced release time, the three present the same release tendency. The release efficiency of Sample-10 has the highest value of 82.9% compared with Sample-3 (73.9%) and Sample-6.5 (78.1%), which should be related with its highest BET surface area and pore size.

The $LaPO_4$:Ce/Tb@Au solution under investigation was irradiated by the UV lamp in a 1 cm length quartz cuvette. During the released period, the comparative samples (with or without irradiation) were shaked together for 1 min at one hour interval. In Fig. S7A, the result indicates the following conclusions: (1) For each release line, there are two steps: the initial fast release which is caused by the diffusion and the following slow value of 7. With the decreased pH value, DOX becomes more positive-charged and the increased electrostatic repulsion release due to the strong interaction between DOX molecules and mesoporous channels of the material. The initially rapid release of drug molecules is essential to the treatment of cancer, because the fast release of anti-cancer drug can inhibit the growth of cancer cells efficiently. After that, the slow release of the rest DOX can be continued for curbing the few survived cells from the first stage. There are 44.1% of DOX molecules released during the initial 1 h without UV irradiation under the pH value of 4. During the remaining release process (1-36 h), 35.4% of DOX is released. (2) The release efficiencies and rates of DOX under pH value of 4 are higher than that under pH makes the drug molecules release faster. For example, there are 79.5% of DOX released under the pH value of 4 while there are only 17.0% released under the pH value of 7. (3) It is found that the released efficiencies (90.9% and 44.4%) under UV irradiation with pH value of 4 and 7 are obviously higher than the efficiencies (82.8% and 17.0%) without UV irradiation. We can see there is an obvious peak at 500-600 nm in the absorbance spectrum of Au NPs solution, which can give rise to photochemical effect caused by the absorbance of Au NPs. The absorbance of the gold particles makes the local temperature increased due to the SPR effect, which reduces the emission intensity but is beneficial to the drug release process with a higher rate.[33]

In order to further prove the thermal effect of the Au NPs under UV light, the release efficiency of $LaPO_4$:Ce/Tb@Au with the UV light on and off during 8 hours was monitored by exposing the solution to alternating hours. Fig. S7B reveals that the release efficiency with the UV light on during the same time interval (1 h) is up to 2 times than that with the light off. The light-dependent rate effectively controls the dose of the released drug with the exposure to UV-light or not. It should be noted that the initial rapid release of DOX molecules is essential to cure cancer, and the slow release of rest drug molecules can be continued for curbing the few survived cells. There is no doubt that the $LaPO_4$:Ce/Tb shows a good drug delivery and release property. Furthermore, the $LaPO_4$:Ce/Tb@Au shows better released properties. More

importantly, the UV light could be potentially used as the regulator to control the released rate and efficiency.

Cellular cytotoxicity is an important factor in evaluating the potential application of the drug delivery system.[34] To investigate the pharmacological activity of the DOX-loaded microspheres, the cytotoxic effect of $LaPO_4$:Ce/Tb@Au-DOX

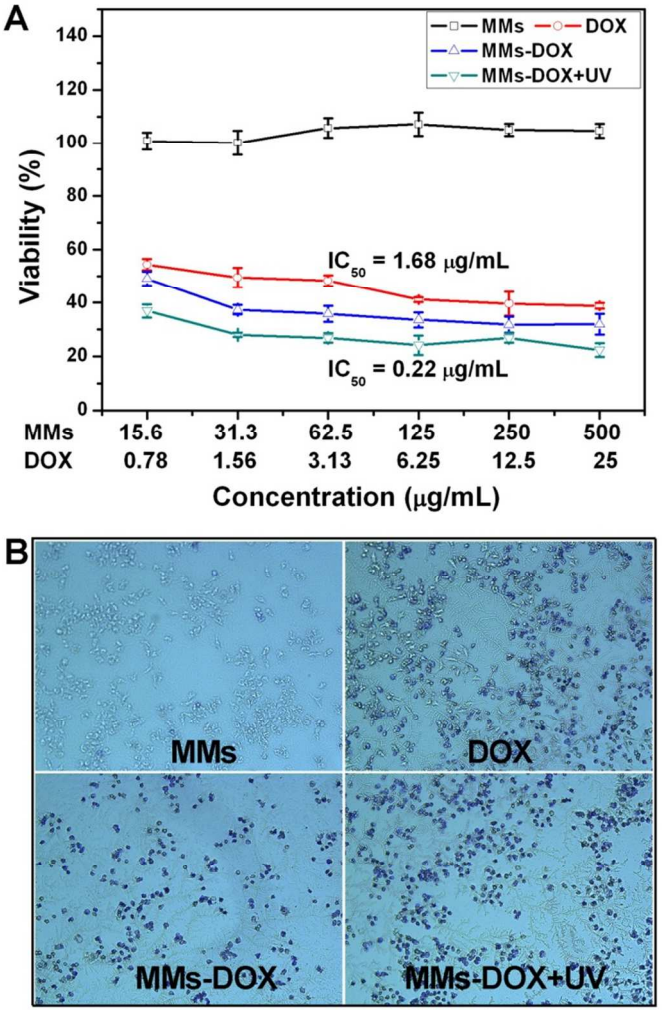

Fig. 9 The viabilities of HeLa cell incubated for 24 h with pure LaPO4:Ce/Tb@Au MMs, free DOX, DOX-$LaPO_4$:Ce/Tb@Au, and DOX-$LaPO_4$:Ce/Tb@Au with UV irradiation with different concentrations (A) and HeLa cells incubated with different groups with trypan blue marked (B).

with and without UV irradiation on HeLa cells was tested *in vitro* via MTT assay. As shown in Fig. 9A, when $LaPO_4$:Ce/Tb@Au MMs was used as the drug carrier, more than 100.4% HeLa cells are viable under a varying concentration range. There are 100.7% cells viable when the concentration is regulated to 500 μg/mL. These results indicate that the $LaPO_4$:Ce/Tb@Au has no cytotoxicity to cells. The cellular viability with free DOX and $LaPO_4$:Ce/Tb@Au MMs-DOX was also investigated. When the concentration of free DOX and $LaPO_4$:Ce/Tb@Au MMs-DOX with the DOX concentration is 25 μg/mL, the viability of the two groups are both lower (38.8% of pure DOX and 31.9% of $LaPO_4$:Ce/Tb@Au MMs-DOX), suggesting that the systems have high cell cytotoxicity when used as the anti-cancer drug carriers. More interestingly, when HeLa cells were incubated with $LaPO_4$:Ce/Tb@Au-DOX under UV irradiation using a UV lamp with the pump power of 0.2 W/cm^2, the MMs composites exhibit higher inhibition against cancer cells, there are only 22.3% of the cancer cells survived with the DOX concentration of 25 μg/mL. The IC_{50} value of MMs-DOX+UV is 0.22μg/mL which is lower than that of pure DOX (1.68 μg/mL).We have also detected the viability of HeLa cells incubated with

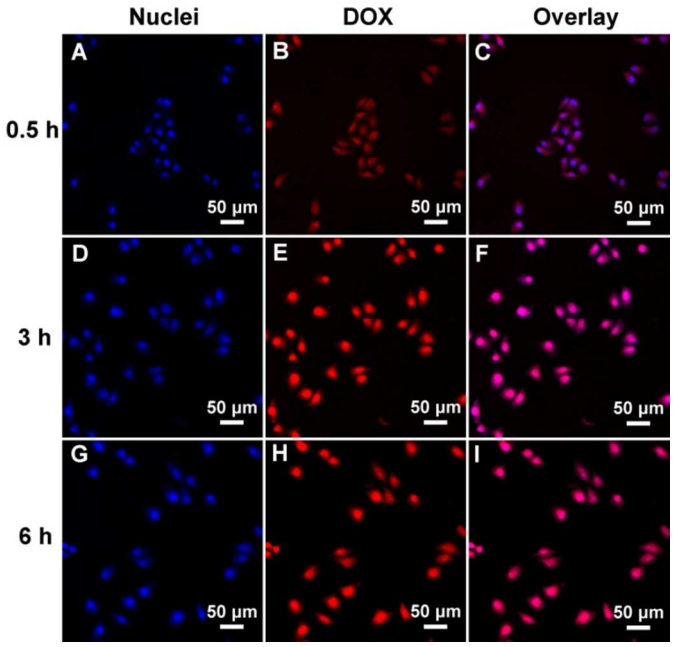

Fig. 10 Confocal laser scanning microscope (CLSM) images of HeLa cells incubated with $LaPO_4$:Ce/Tb@Au-DOX MMs for 0.5 h (A-C) and 3 h (D-F).

different groups dyed with trypan blue. As shown in Fig. 9B, the viability of the HeLa cells decreased incubated with culture only, pure DOX, MMs-DOX, and MMs-DOX with UV irradiation. HeLa cells are almost wholly dead in the last group which is well coincident with MTT assay. In conclusion, the DOX-$LaPO_4$:Ce/Tb@Au under UV light with strong curbing effect to cancer cells is due to the combined thermal-effect of the MMs and chemo-effect of DOX.[36]

In addition, we also detected the cell up-taken properties incubated with $LaPO_4$:Ce/Tb@Au-DOX dyed by DAPI using confocal laser scanning microscope (CLSM) (Fig. 10). The excitation wavelength of DOX is 552 nm and the DOX emissions were used to mark the $LaPO_4$:Ce/Tb@Au-DOX composite. There are blue emissions emitted by DAPI in the nuclei and red emissions emitted by DOX. Fig. 10 indicates that $LaPO_4$:Ce/Tb@Au-DOX are evident in the intracellular region, and no luminescent signal outside of cells is measured, suggesting that the MMs have been internalized into the cells rather than merely staining the membrane surface.[37] Meanwhile, with enhancement of the incubation time, the red emissions of DOX increase, indicating that more and more MMs are taken up by the cells. These observations demonstrate that the as-prepared MMs are promising candidates as anti-drug carriers.

As a proof of principle experiments, the H22 tumor-bearing mice were intratumor injection of DOX and MMs-DOX. Fig. 11A shows the yellow-green DC luminescent emissions under the UV irradiation which indicates the MMs could be utilized as bio-imaging carriers for potential diagnoses. The mice were investigated when the tumor size grew to 6-8 mm. After different treatment, the results are different. In Fig. 11B and

11C, the size of tumor is very large without any injection (about 28 mm) and smaller with DOX injected (about 18 mm). With the MMs-DOX injected under UV irradiation, the tumor is inhibited mostly to some extent (about 10 mm). Besides that, the sizes of mice body kept increase without other abnormal phenomenon. H&E stained images of tumor in Fig. 11D, there

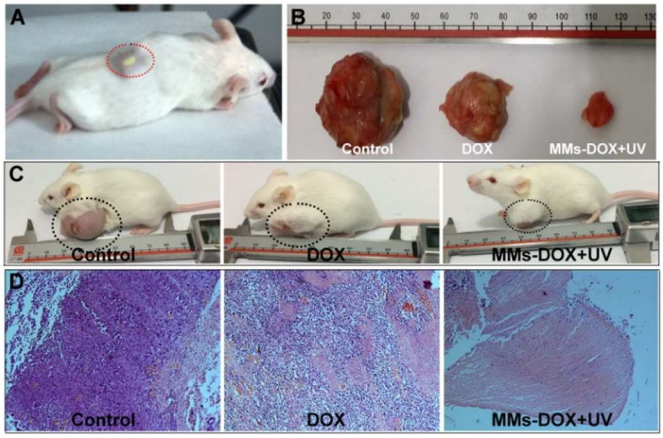

Fig. 11 DC luminescent image of a tumor-bearing mouse after injection of MMs (A). Representative photographs of H22 tumors (B), mice (C), H&E stained images of tumors (D) after various treatments: with nothing, pure DOX, MMs-DOX with UV irradiation, and photographs of tumor tissue were obtained after 14 days.

are obvious degenerative changes of coagulative necrosis with karyorrhectic debris and marked karyolysis included were found in control group. What is more, almost all of tumor cells were severely destroyed in the MMs-DOX+UV group. The result indicates most tumor cells treated with MMs-DOX under UV laser irradiation were destroyed and inhibited compared to the control group. Meanwhile, histological analysis of the heart, lung, kidney, liver, and spleen were shown in Figure S8 which indicates the groups treated with MMs-DOX under UV irradiation present good result. In the control group, necrosis was found in the histological samples, and there are symptoms of inflammation and glomerulus atrophy. Compared with the controlled group, the organs with best treated show the following result: Hepatocytes in the liver samples were found normal; No pulmonary fibrosis was detected in all the lung samples; The glomerulus structure in the kidney section was observed clearly. These results clearly demonstrate the potential clinical applicability of $LaPO_4$:Ce/Tb@Au MMs as anti-tumor carriers.

4. Conclusions

In summary, we have prepared uniform $LaPO_4$:Ce/Tb and $LaPO_4$:Ce/Tb@Au MMs constituted of numerous nanorods by a large-scale and mild co-precipitation route. The as-prepared $LaPO_4$:Ce/Tb@Au MMs have a BET surface area of 66.2 m^2/g. Under UV excitation, $LaPO_4$:Ce/Tb and $LaPO_4$:Ce/Tb@Au MMs emit the characteristic green emissions of Tb^{3+} ions. During the DOX process, the photothermal effect of Au NPs results in a rapid DOX release from the Au hybrid materials under UV irradiation. MTT assay and hemolysis result indicates the good biocompatibility on L929 cells and obvious cytotoxic effect on cancer cells of this system. Furthermore, the cytotoxicity incubated with the cancer cells under the UV irradiation further proved the strong inhibition against the cancer cells due to the thermal effect of Au NPs. The CLSM images, the anti-cancer properties *in vivo*, and the histology examination proved the potential candidate as anti-cancer drug carrier with bio-imaging.

Acknowledgements

This work was supported by funding from financial supports from the National Natural Science Foundation of China (NSFC 21271053, 21401032, 51472058), Research Fund for the Doctoral Program of Higher Education of China (2011230411002), Natural Science Foundation of Heilongjiang Province (B201403), Harbin Sci.-Tech. Innovation Foundation (RC2012XK017012, 2014RFQXJ019) and Fundamental Research Funds for the Central Universities of China (HEUCF201403006).

Notes and references

Key Laboratory of Superlight Materials and Surface Technology, Ministry of Education, College of Materials Science and Chemical Engineering, Harbin Engineering University, Harbin 150001, P. R. China. E-mail: yangpiaoping@hrbeu.edu.cn; gaishili@hrbeu.edu.cn

† Electronic Supplementary Information (ESI) available: [UV-vis absorption spectrum and calibration curve of DOX solution, XRD patterns of $LaPO_4$ and $LaPO_4$:Ce/Tb, TEM image of the $La(OH)CO_3$:Ce/Tb precursor, SEM image of the as-prepared $LaPO_4$:Ce/Tb@Au MMs and the diameter distribution diagrams of the precursor and $LaPO_4$:Ce/Tb@Au, The absorption spectrum of gold nano-particle solution, Nitrogen adsorption/desorption isotherm and the DOX release efficiency of $LaPO_4$:Ce/Tb MMs with different initial pH values, DOX release efficiency of $LaPO_4$:Ce/Tb@Au MMs and the release efficiency with and without the UV irradiation, H&E stained images of mice heart, liver, spleen, lung, and kidney organs treated with different groups: control, pure DOX, and $LaPO_4$:Ce/Tb@Au MMs-DOX with UV irradiation.]. See DOI: 10.1039/b000000x/

1 S. Gai, C. Li, P. Yang and J. Lin, *Chem. Rev*, 2013, **114**, 2343.
2 Y. Chen, J. Wang, C. M. Liu, J. K. Tang, X. J. Kuang, M. M. Wu, Q. Su, *Opt. Express*, 2013, **21**, 3161; J. W. Stouwdam and F. van Veggel, *Langmuir*, 2004, **20**, 11763; X. Z. Xiao, B. Yan, *J. Am. Ceram. Soc*. 2010, **93**, 2195.
3 P. Dorenbos, *J. Lumin.,* 2005, **111**, 89; L. Y. Zhang, T. T. Wang, L. Yang, C. Liu, C. G. Wang, H. Y. Liu, Y. A. Wang and Z. M. Su, *Chem. Eur. J.*, 2012, **18**, 12512; L. Zhou, Z. Chen, K. Dong, M. Yin, J. Ren and X. Qu, *Adv. Mater.*, 2014, **26**, 2424.
4 Q. He, and J. Shi, *J. Mater. Chem.* 2011, **21**, 5845; Y. Liu, D. Tu, H. Zhu and X. Chen, *Chem. Soc. Rev.*, 2013, **42**, 6924; Z. Chen, H. Chen, H. Hu, M. Yu, F. Li, Q. Zhang, Z. Zhou, T. Yi and C. Huang, *J. Am. Chem. Soc.*, 2008, **130**, 3023.
5 D. Brevet, M. Gary-Bobo, L. Raehm, S. Richeter, O. Hocine, K. Amro, B. Loock, P. Couleaud, C. Frochot, A. Morere, P. Maillard, M. Garcia and J.-O. Durand, *Chem. Commun.*, 2009, **12**, 1475.
6 Slowing, II, B. G. Trewyn, S. Giri and V. S. Y. Lin, *Adv. Funct. Mater.*, 2007, **17**, 1225; Y. Lin, J. Ren and X. Qu, *Acc. Chem. Res.*, 2014, **47**, 1097.
7 F. Torney, B. G. Trewyn, V. S. Y. Lin and K. Wang, *Nat. Nanotechnol.*, 2007, **2**, 295; Chen, C., Nan, C., Wang, D., Su, Q., Duan, H., Liu, X., Zhang, L., Chu, D., Song, W., Peng, Q. and Li, Y., *Angew. Chem. Int. Ed.*, 2011, **50**, 3725; S. Zhang, W. Ni, X. Kou, M. H. Yeung, L. Sun, J. Wang and C. Yan, *Adv. Funct. Mater.*, 2007, **17**, 3258.
8 S. Gallini, J. R. Jurado and M. T. Colomer, *Chem. Mater.*, 2005, **17**, 4154.

9 S. Hachani, B. Moine, A. El-akrmi and M. Ferid, *Opt. Mater.*, 2009, **31**, 678; W. B. Park, S. P. Singh, M. Pyo and K.-S. Sohn, *J. Mater. Chem.*, 2011, **21**, 5780.

10 L. H. Zhang, M. L. Yin, H. P. You, M. Yang, Y. H. Song and Y. J. Huang, *Inorg. Chem.,* 2011**, 50**, 10608; W. B. Bu, Z. Hua, H. R. Chen and J. L. Shi, *J. Phys. Chem. B*, 2005, **109**, 14461.

11 M. Yu, H. Wang, C. K. Lin, G. Z. Li and J. Lin, *Nanotechnology,* 2006**,** *17*, 3245; W. Li and J. Lee, *J. Phys. Chem. C*, 2008, **112**, 11679.

12 L. Zhu, X. M. Liu, X. D. Liu, Q. Li, J. Y. Li, S. Y. Zhang, J. Meng and X. Q. Cao, *Nanotechnology*, 2006, **17**, 4217.

13 Z. Y. Hou, L. L. Wang, H. Z. Lian, R. T. Chai, C. M. Zhang, Z. Y. Cheng and J. Lin, *J. Solid. State. Chem.*, 2009, **182**, 698.

14 M. Yang, H. P. You, K. Liu, Y. H. Zheng, N. Guo and H. J. Zhang, *Inorg. Chem.*, 2010, **49**, 4996; E. E. Boakye, P. Mogilevsky and R. S. Hay, *J. Am. Ceram. Soc.*, 2005, **88**, 2740.

15 M. Fernandes, V. d. Z. Bermudez, R. A. S. Ferreira, L. D. Carlos, A. Charas, J. Morgado, M. M. Silva and M. J. Smith, *Chem. Mater.*, 2007, **19**, 3892; Y. Liu, S. Zhou, D. Tu, Z. Chen, M. Huang, H. Zhu, E. Ma and X. Chen, *J. Am. Chem. Soc.*, 2012, **134**, 15083–15090.

16 L. X. Yu, H. W. Song, S. Z. Lu, Z. X. Liu, L. M. Yang and X. G. Kong, *J. Phys. Chem. B*, 2004, **108**, 16697; L. X. Yu, H. W. Song, Z. X. Liu, L. M. Yang and S. Zheng, *J. Phys. Chem. B*, 2005, **109**, 11450.

17 T.-S. Chan, C.-L. Dong, Y.-H. Chen, Y.-R. Lu, S.-Y. Wu, Y.-R. Ma, C.-C. Lin, R.-S. Liu, J.-L. Chen, J. Guo, J.-F. Lee, H.-S. Sheu, C.-C. Yang and C.-L. Chen, *J. Mater. Chem*., 2011, **21**, 17119; R.-S. Liu, Y.-H. Liu, N. C. Bagkar and S.-F. Hu, *Appl. Phys. Lett.*, 2007, **91**, 061119; H. Liu, W. Lu, H. Wang, L. Rao, Z. Yi, S. Zeng and J. H. Hao, *Nanoscale*, 2013, **5**, 6023; M. N. Luwang, R. S. Ningthoujam, Jagannath, S. K. Srivastava and R. K. Vatsa, *J. Am. Chem. Soc.*, 2010, **132**, 2759; Y. S. Liu, D. T. Tu, H. M. Zhu, R. F. Li, W. Q. Luo and X. Y. Chen, *Adv. Mater.*, 2010, **22**, 3266; F. Wang, R. Deng, J. Wang, Q. Wang, Y. Han, H. Zhu, X. Chen and X. Liu, *Nat. Mater.*, 2011, **10**, 968; X. F. Yang, I. D. Williams, J. Chen, J. Wang, H. F. Xu, H. M. Konishi, Y. X. Pan, C. L. Liang and M. M. Wu, *J. Mater. Chem.*, 2008**, 18**, 3543; A. K. Sharma, K. H. Son, B. Y. Han and K. S. Sohn, *Adv. Funct. Mater.*, 2010**, 20**, 1750.

18 D. Peer, J. M. Karp, S. Hong, O. C. FaroKhzad, R. Margalit and R. Langer, *Nat. Nanotechnol*., 2007, **2**, 751; Y. Fan, C. Li, H. Cao, F. Li and D. Chen, *Biomaterials*, 2012**, 33**, 4220; Q. Lin, Q. Huang, C. Li, C. Bao, Z. Liu, F. Li and L. Zhu, *J. Am. Chem. Soc*., 2010, **132**, 10645.

19 Q. Zhao, F. Li and C. Huang, *Chem. Soc. Rev.*, 2010, **39**, 3007; L. P. Liu, G. M. Wang, Y. Li, Y. D. Li and J. Z. Zhang, *Nano Res.*, 2011, **4**, 249.

20 L. D. Carlos, R. A. S. Ferreira, V. d. Z. Bermudez and S. J. L. Ribeiro, *Adv. Mater.*, 2009, **21**, 509; Y. Zhang and J. H. Hao, *J. Mater. Chem. C*, 2013, **1**, 5607; M. Chen, Z. Lei, W. Feng, C. Li, Q.-M. Wang and F. Li, *Biomaterials*, 2013, **34**, 4284; J. Bao, W. Chen, T. Liu, Y. Zhu, P. Jin, L. Wang, J. Liu, Y. Wei and Y. Li, *ACS Nano*, 2007, **1**, 293.

21 N. Liu, W. Qin, G. Qin, T. Jiang and D. Zhao, *Chem. Commun.*, 2011, **47**, 7671.

22 Y. W. Xu, Y. H. Ni, X. Ma and J. M. Hong, *CrystEngComm*, 2013, **15**, 271.

23 G. Phaomei, R. S. Ningthoujam, W. R. Singh, R. S. Loitongbam, N. S. Singh, A. Rath, R. R. Juluri and R. K. Vatsa, *Dalton Trans.*, 2011, **40**, 11571.

24 I. F. Li, C. H. Su, H. S. Sheu, H. C. Chiu, Y. W. Lo, W. T. Lin, J. H. Chen and C. S. Yeh, *Adv. Funct. Mater.,* 2008, **18**, 766; A. Kar, A. Kundu, S. Bhattacharyya, S. Mandal and A. Patra, *RSC Adv.*, 2013, **3**, 13372.

25 K. Rajesh, P. Mukundan, P. K. Pillai, V. R. Nair and K. G. K. Warrier, *Chem. Mater.*, 2004, **16**, 2700.

26 S. L. Gai, P. P. Yang, P. A. Ma, D. Wang, C. X. Li, X. B. Li, N. Niu and J. Lin, *J. Mater. Chem.*, 2011, **21**, 16420.

27 W. H. Di, X. G. Ren, H. F. Zhao, N. Shirahata, Y. Sakka and W. P. Qin, *Biomaterials*, 2011, **32**, 7226.

28 P. Yang, S. Gai and J. Lin, *Chem. Soc. Rev.*, 2012, **41**, 3679.

29 Q. Ju, W. Luo, Y. Liu, H. Zhu, R. Li and X. Chen, *Nanoscale*, 2010, **2**, 1208.

30 J. Yang, C. Li, Z. Quan, C. Zhang, P. Yang, Y. Li, C. Yu and J. Lin, *J. Phys. Chem. C*, 2008, **112**, 12777; L. Wang, Z. Hou, Z. Quan, C. Li, J. Yang, H. Lian, P. Yang and J. Lin, *Inorg. Chem.*, 2009, **48**, 6731.

31 M. Long, F. S. Hong, W. Li, F. C. Li, H. Y. Zhao, Y. Q. Lv, H. X. Li, F. Hu, L. D. Sun, C. H. Yan and Z. G. Wei, J. Lumin., 2008, **128**, 428.

32 Y. L. Dai, D. M. Yang, P. A. Ma, X. J. Kang, X. Zhang, C. X. Li, Z. Y. Hou, Z. Y. Cheng and J. Lin, *Biomaterials*, 2012, **33**, 8704.

33 H. He, C. Xie and J. Ren, *Anal. Chem.,* **2008,** *80*, 5951; S. S. Agasti, A. Chompoosor, C.-C. You, P. Ghosh, C. K. Kim and V. M. Rotello, *J. Am. Chem. Soc*., 2009, **131**, 5728.

34 X. J. Kang, Z. Y. Cheng, C. X. Li, D. M. Yang, M. M. Shang, P. A. Ma, G. G. Li, N. A. Liu and J. Lin, *J. Phys. Chem. C*, 2011, **115**, 15801.

35 G. S. Yi and G. M. Chow, *J. Mater. Chem.*, 2005, **15**, 4460.

36 Y. Dai, H. Xiao, J. Liu, Q. Yuan, P. a. Ma, D. Yang, C. Li, Z. Cheng, Z. Hou, P. Yang and J. Lin, *J. Am. Chem. Soc.*, 2013, **135**, 18920.

37 P. Huang, W. Zheng, S. Zhou, D. Tu, Z. Chen, H. Zhu, R. Li, E. Ma, M. Huang and X. Chen, *Angew. Chem. Int. Ed.*, 2014, **53**, 1252, L. Cheng, K. Yang, Y. Li, J. Chen, C. Wang, M. Shao, S.-T. Lee and Z. Liu, *Angew. Chem. Int. Ed*., 2011, **50**, 7385.

